Cent. Eur. J. Eng. • 2(4) • 2012 • 585-602
DOI: 10.2478/s13531-012-0035-z

VERSITA

Central European Journal of **Engineering**

Modelling and analysis of vehicle crash system integrated with different VDCS under high speed impacts

Research Article

Mustafa Elkady[1,2*], Ahmed Elmarakbi[2]

1 Department of Computing, Engineering and Technology, University of Sunderland, The Sir Tom Cowie Campus at St Peter's, St Peter's Way, Sunderland, SR6 0DD, UK

2 Department of Automotive Engineering, Faculty of Engineering, Ain Shams University, Cairo, Egypt

Received 28 April 2012; accepted 4 August 2012

Abstract: The behaviour of a vehicle at high-speed crashes is enhanced by using active vehicle dynamics control systems. A 6-Degree-of-Freedom (6-DOF) mathematical model is developed to carry out this study. In this model, vehicle dynamics is studied together with vehicle crash structural dynamics. Validation of the vehicle crash structure of the proposed model is achieved to ensure that the modelling of the crumble zone and the dynamic responses are reliable. Five different speeds are selected to investigate the robustness of control system and its effect on the vehicle crash characteristics at low and high speeds with full and offset collision scenarios. A great improvement of vehicle pitch and yaw angels and accelerations at high speed collision are obtained from this analysis.

Keywords: Active safety• Collision mitigation• High speed collision• Vehicle dynamics control• Mathematical modelling• Numerical simulations

1. Introduction

During the past decades, many crash avoidance devices such as turn seatbelts and airbags have been installed in vehicles to protect the occupant by absorbing the energy caused by a crash. Furthermore, to improve the vehicle crash energy absorption capability, the vehicle's front-end and side structures have been developed and enhanced. However, the collision speed still is very important for the crash outcome. At a collision speed of 80 km/h, the possibility that the car occupants are killed is about 20 times greater than at a speed of 30 km/h [1].

ADAS techniques have been investigated in an endeavour to alleviate vehicle crash [2–6]. The main purpose of the ADAS is to warn the driver of dangerous situations and aid him actively in an impending collision. However, ADAS has yet to achieve their goal to prevent vehicle collision. With regard to the occupant safety, vehicle body pitch and drop during frontal impact play an important role in injuries to the driver's neck and head [7–9]. Vehicle body pitch and drop have normally been experienced in frontal crash tests. A finite element (FE) method has been used to investigate frame deformation upon full-frontal impact and to discuss the cause and counter-measures design regarding vehicle

*E-mail: bf41xb@student.sunderland.ac.uk

body pitch and drop [7]. It was found that downward bending generated from the geometric offsets of the frame rails in the vertical direction during a crash is the key feature of vehicle body pitching.

The development of the vehicle dynamics control systems (VDCS) plays an important role in improving vehicle stability, ride characteristics and passenger safety. The anti-lock braking system (ABS) and the yaw moment control system are used to assist vehicle stability during emergency manoeuvres, while the active suspension control system (AS) is used to improve vehicle ride quality and reduce the vehicle vertical acceleration [10, 11]. In addition, the AS control system integrated with the ABS is used to reduce the vehicle stopping distance [12].

Very little research has been carried out to investigate the effect of the VDCS on vehicle collision. The influence of the braking force on vehicle impact dynamics in low-speed rear-end collisions has been studied [13]. It was confirmed that the braking force was not negligible in high-quality simulations of vehicle impact dynamics at low speed. The effect of vehicle braking, anti-pitch control system, and direct yaw control (DYC) on vehicle crash routine (at vehicle speeds of 55 km/hr) was investigated using ADAMS multibody dynamics model [14]. Hogan's study found that the ABS has a detrimental effect on vehicle crash performance during offset barrier impacts while DYC systems proved to significantly improve performance in vehicle-to-vehicle collision. However, he mentioned that more research into the effect of VDCS on vehicle collision mitigation is recommended.

In this paper, a new 6-Degree-of-Freedom (6-DOF) vehicle dynamics/crash mathematical model has been developed to improve the vehicle collision performance at high speed collisions in full and offset frontal crash scenarios. The ABS and the AS control system are co-simulated with the mathematical model. The AS control system is used to reduce vehicle body pitch angle, pitch acceleration, yaw angle, and yaw acceleration.

2. Car model

In this section, a 6-DOF vehicle dynamics/crash mathematical model has been presented and is used to implement this study. Using mathematical models in crash simulations is useful at the first design concept, because rapid analysis is required at this stage. In addition, the well-known advantage of mathematical modelling provides a quick and valid simulation analysis compared with finite element models.

Vehicle crash structures are designed to be able to absorb the crash energy and control vehicle deformations; therefore simple mathematical models have been used to represent the vehicle front structure [15]. In this model, vehicle mass is represented by lumped mass and vehicle structure is represented by a spring in a simple model to simulate frontal and rear-end vehicle collision processes. Moreover, other analyses and simulations of vehicle-to-barrier impact using a simple mass spring model were established by Kamal [16]. Kamal's study demonstrated that mathematical modelling can be accurately used for unlimited numbers of vehicle-to-barrier crash tests. To achieve enhanced occupant safety, the crash energy management system was investigated by Khattab [17]. This study, using a simple lumped-parameter model, discussed the applicability of providing variable energy absorbing properties as a function of the impact speed.

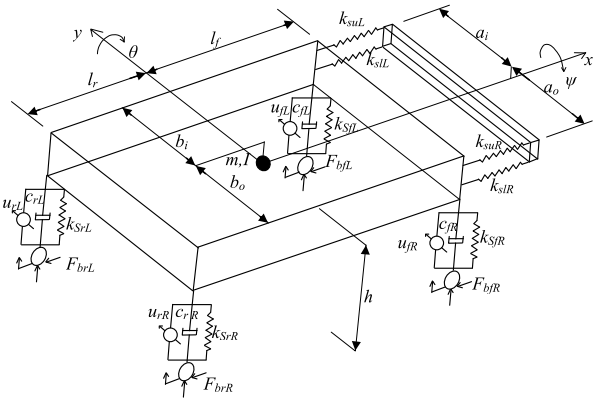

Figure 1. 6-DOF Vehicle Dynamics/Crash Mathematical Model.

The 6-DOF model used in this paper is developed to optimize the VDCS in impending impact at full and offset crash scenarios. The ABS and the AS control systems are co-simulated with a full car vehicle dynamic model and integrated with a non-linear front-end structure model as shown in Figure 1. Figures 2(a) and 2(b) are the pitch-plane and yaw-plane of the mathematical model, which are used to clarify and simplify the 3-D drawing. It is assumed that the front-end springs are still horizontal during impact and they will not incline with the vehicle body.

In this model, the vehicle body is represented by lumped mass m and four spring/damper units are used to represent the vehicle suspension system. The AS system is co-simulated with the suspension system and the ABS is co-simulated with the model using a simple wheel model. Four nonlinear springs are also proposed to represent the upper and lower members of the vehicle frontal structure. The mass of the impacted part of the bumper is neglected because it is not moving during collision, while the mass of the rotational part of the bumper requires consideration. It is assumed that the vehicle moves on a flat asphalted road, thus neglecting the vertical movement of the tyres and

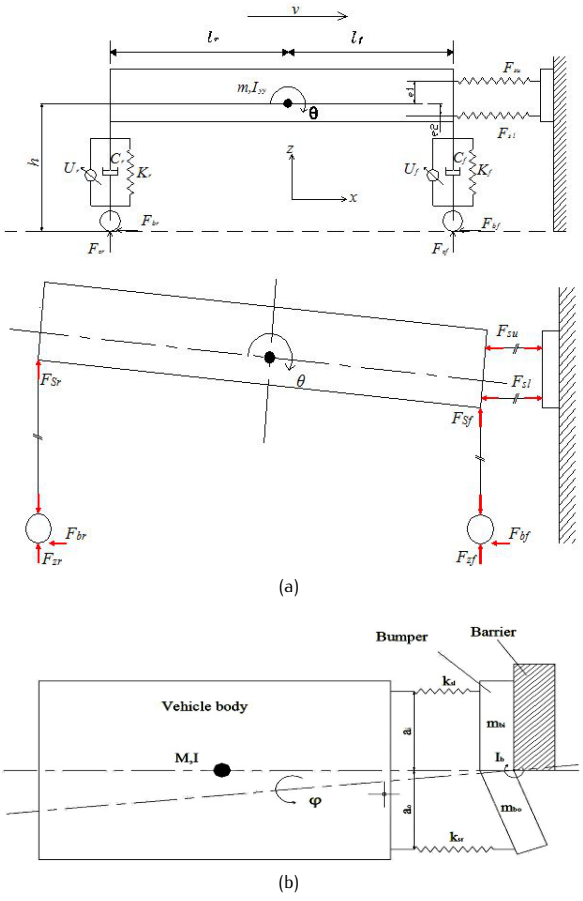

Figure 2. (a) pitch-plane view and its free-body diagram; (b) yaw-plane view and its free-body diagram.

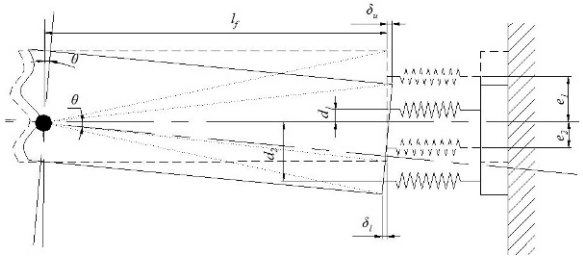

Figure 3. Illustration drawing of the front-end deformation due to vehicle pitching (--- before pitching, — after pitching).

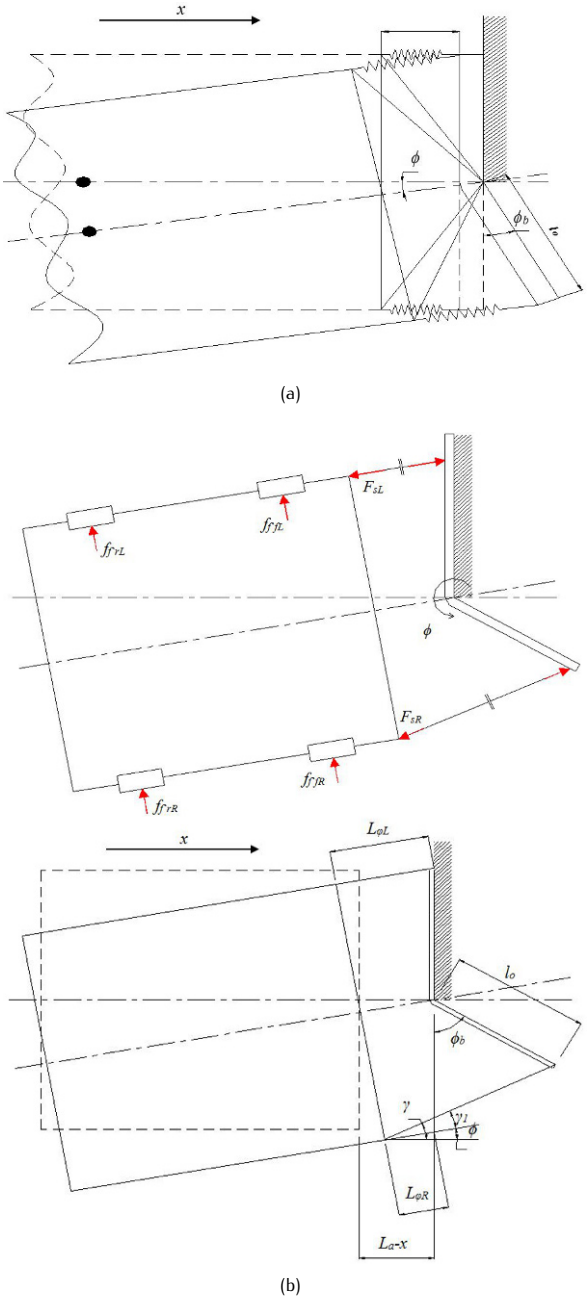

Figure 4. (a) illustration drawing of the front-end deformation due to vehicle yawing (--- before yawing, — after yawing); (b) simplification of Figure 4(a) and its free-body diagram.

road vertical forces. Vehicle body pitching is due to vehicle braking, the different values between the upper and lower crash forces, and the different distances between upper and lower members from the vehicle's centre of gravity.

2.1. Equation of motion of the mathematical model

In this section, the mathematical model and its equations of motion are developed to study and predict the dynamic response of the primary impact in full and offset vehicle-to-barrier crash scenarios. Figure 3 shows the deformation of

the front springs due to vehicle pitching; Figure 4 shows the deformation of the front springs due to vehicle rotation around the point of impact. The equations of motion of the 6-DOF model can be written using Figures 1, 3 and 4 as:

$$m \cdot \ddot{x} + (F_{suR} + F_{slR}) \cdot \cos\gamma + (F_{suL} + F_{slL}) \cdot \cos\phi + F_{bfR} + F_{brR} + F_{brL} = 0 \quad (1)$$

$$m \cdot \ddot{z} + F_{SfR} + F_{SfL} + F_{SrR} + F_{SrL} = 0 \quad (2)$$

$$I_{yy} \cdot \ddot{\theta} - (F_{SfR} + F_{SfL}) \cdot l_f + (F_{SrR} + F_{SrL}) \cdot l_r + (F_{SuR} \cdot \cos\gamma + F_{SuL} \cdot \cos\phi) \cdot d_1 - (F_{slR} \cdot \cos\gamma + F_{slL} \cdot \cos\phi) \cdot d_2 - (F_{bfR} + F_{bfL} + F_{brR} + F_{brL}) \cdot (z + h) = 0 \quad (3)$$

$$I_{zz} \cdot \ddot{\phi} + (F_{suR} + F_{slR}) \cdot \cos\gamma_1 \cdot a_o - (F_{suL} + F_{slL}) \cdot a_i - (F_{suR} + FslR) \cdot \sin\gamma_1 \cdot (l_a - x) + (F_{bfR} + F_{brR}) \cdot b_o - (F_{bfL} + F) \cdot b_i + (F_{f'fR} + F_{f'fL}) \cdot (l_b - x) + (F_{f'rR} + F_{f'rL}) \cdot (l + l_b - x) = 0 \quad (4)$$

$$I_{xx} \cdot \ddot{\psi} + (F_{SfL} + F_{SrL}) \cdot b_i - (F_{SfR} + F_{SrR}) \cdot b_i - (F_{ff'R} + F_{ff'L} + F_{f'rR} + F_{f'rL}) \cdot (z + h) - F_{suR} \sin\gamma_1 \cdot e_1 + F_{slR} \sin\gamma_1 \cdot e_2 = 0 \quad (5)$$

$$I_{zzb} \cdot \ddot{\phi}_b - (FsuR + F_{slR}) \cos\gamma \cdot l_o \cos\phi_b - (F_{suR} + F_{slR}) \sin\gamma \cdot l_o \sin\phi_b = 0 \quad (6)$$

where m, I_{yy}, I_{xx} and I_{zzb} are the mass of the vehicle body, the moment of inertia of the vehicle body about the y axis, the moment of inertia of the vehicle body about the x axis, the moment of inertia of the vehicle body about z axis at the point of impact and the moment of inertia of the rotation part of the bumper about the z axis at the point of impact, respectively. $\ddot{x}$ and $\ddot{z}$ are the acceleration of the vehicle body in longitudinal direction and the acceleration of the vehicle body in the vertical direction, respectively. $\ddot{\theta}$, $\ddot{\phi}$, $\ddot{\psi}$ and $\ddot{\phi}_b$ are the rotational pitching, yawing, rolling acceleration of the vehicle body, and rotational acceleration of the rotation part of the bumper, respectively. x and z are the vehicle body longitudinal and vertical displacements, respectively. F_s, F_b, F_S and $F_{f'}$ are the front-end non-linear spring forces, the braking forces, the vehicle suspension forces and the friction forces between the tyres and the road due to vehicle yawing, respectively. As shown in Figure 4(b), ϕ, ϕ_b, γ and γ_1 represent the vehicle body yaw angle, the rotational part of the bumper angle, the angle between the front-end right springs and x axis and the difference angle between φ and γ, respectively. l_f, l_r, l and h represent the longitudinal distance between the vehicle centre of gravity (CG) and front wheels, the longitudinal distance between the CG and rear wheels, the wheel base and the CG height, respectively. a_i and a_o are the distance between the point of impact and impacted springs and the distance between the point of impact and non-impacted springs, respectively. b_o and b_i are the distance between the CG and right wheels, the CG and left wheels, respectively.

The front-end springs' location is represented by the subscripts u_R, u_L, l_R and l_L which denote upper right spring, upper left spring, lower right spring and lower left spring, respectively. The vehicle wheel location is represented by the subscripts f_R, f_L, r_R and r_L which denote front right wheel, front left wheel, rear right wheel and rear left wheel, respectively. l_a, l_b, l_o, e_1 and e_2 represent the length of the front-end springs, the distance between the bumper and the centre of front wheels, the distance between the point of impact and the end of rotational part of the bumper, the distance between the CG and front-end upper springs and the CG and front-end lower springs, respectively. It should be noted that at full frontal collision the distance l_o is equal to zero and equations 3, 4 and 5 are eliminated. d_1 and d_2 represent the distance between the CG and the upper springs force and the CG and the lower springs force, respectively, and can be calculated using Figure 3 as:

$$d_1 = \sqrt{l_f^2 + e_1^2} \cdot \sin\left(\tan^{-1}\left(\frac{e_1}{l_f}\right) - \theta\right) \quad (7)$$

$$d_2 = \sqrt{l_f^2 + e_2^2} \cdot \sin\left(\tan^{-1}\left(\frac{e_2}{l_f}\right) - \theta\right) \quad (8)$$

angles γ and γ_1 can be calculated as shown in Figure 4(b) by:

$$\gamma = \tan^{-1}\left(\frac{l_o - l_o\cos\phi_b}{l_o \cdot \sin\phi_b + l_{\phi R} \cdot \cos\phi}\right) \quad (9)$$

$$l_{\phi R} = \frac{(l_a - x) - a_o \sin\phi}{\cos\phi} \quad (10)$$

$$\gamma_1 = \gamma - \phi \quad (11)$$

2.2. Forces generated by the suspension system

The suspension forces are generated via vertical movement of the vehicle body and depend on the displacement and

velocity of the body motion and can be written as follows:

$$F_{SfR} = k_{SfR}(z - l_f \cdot \sin\theta - b_o \cdot \psi) + c_{fR}(\dot{z} - l_f \cdot \dot{\theta} \cdot \cos\theta - b_o \cdot \dot{\psi}) - u_{fR} \quad (12)$$

$$F_{Sfl} = k_{SfL}(z - l_f \cdot \sin\theta - b_i \cdot \psi) + c_{fL}(\dot{z} - l_f \cdot \dot{\theta} \cdot \cos\theta - b_i \cdot \dot{\psi}) - u_{fL} \quad (13)$$

$$F_{SrR} = k_{SrR}(z - l_r \cdot \sin\theta - b_o \cdot \psi) + c_{rR}(\dot{z} - l_r \cdot \dot{\theta} \cdot \cos\theta - b_o \cdot \dot{\psi}) - u_{rR} \quad (14)$$

$$F_{SrL} = k_{SrL}(z - l_r \cdot \sin\theta - b_i \cdot \psi) + c_{rL}(\dot{z} - l_r \cdot \dot{\theta} \cdot \cos\theta - b_i \cdot \dot{\psi}) - u_{rL} \quad (15)$$

where k_S, c and u represent the stiffness of the suspension springs, the damping of the suspension coefficients and the active suspension force elements, respectively. θ and ψ are the vehicle body pitching and rolling angels, respectively. $\dot{z}$, $\dot{\theta}$ and $\dot{\psi}$ represent the vehicle body vertical velocity, pitching velocity and rolling velocity, respectively.

2.3. Forces generated by the control systems

The ABS and AS control systems are co-simulated with the mathematical model. To calculate the braking force generated from the ABS, a simple wheel-road model shown in Figure 5(a) is used, and its associated equation can be written as:

$$I\dot{\omega} = T_w - T_{bk} - F_{bk} \cdot r_w - T_{bk} \quad (16)$$

$$F_{bk} = \mu(\lambda) \cdot F_{zk} \quad (17)$$

the slip ratio λ is defined as:

$$\lambda = \frac{v - v_w}{v} = \frac{v - \omega \cdot r_w}{v} \quad (18)$$

the relationship between $\mu(\lambda)$ and wheel slip λ is shown in Figure 5(b), which can be approximated by the following function (Ting & Lin 2004):

$$\mu(\lambda) = 2\mu_o \frac{\lambda_o \lambda}{\lambda_o^2 + \lambda^2} \quad (19)$$

where I is the wheel moment of inertia, ω is the wheel angular velocity, $\dot{\omega}$ is the wheel angular acceleration, T_w is the friction torque, T_b is the braking torque applied by the disk/drum brakes, r_w is the wheel radius, μ is the friction coefficient between the tyre and the road, λ is the tyre slip ratio, λ_o is the optimal slip ratio, which can yield the peak friction value $\mu(\lambda_o) = \mu_o$, F_z is the vertical normal forces of the tyres, v is the vehicle body velocity, and v_w is the equivalent wheel longitudinal velocity. The subscript k indicates the wheel's location (f_R: front right wheel, f_L: front left wheel, r_R: rear right wheel and r_L: rear left wheel). The wheel rotational angle can be calculated after the integration of Equation (1), and then the estimation of the slip ratio λ can be driven. The values of the slip ratio are then used to feed the ABS controller. This controller compares the error between the desired slip ration (from 0.18 to 0.3) and the estimated one. Relative to the error comparison, the ABS controller turns the brake on/off which controls the braking torque T_b to sustain the coefficient of friction μ at its maximum values (μ_o), therefore the maximum braking force can be obtained.

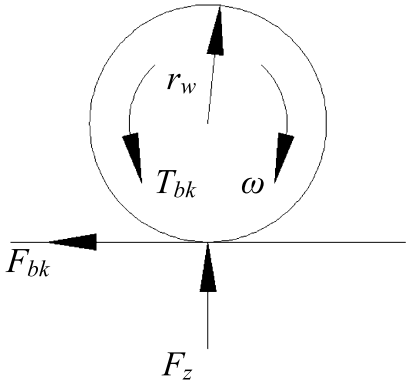

(a) (Ting & Lin 2004)

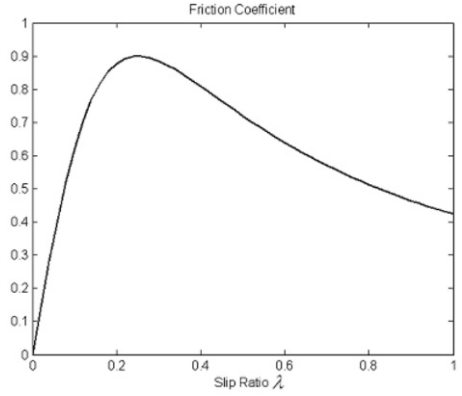

(b) (Ting & Lin 2004)

Figure 5. (a) wheel-road model; (b) the relationship between friction coefficient and wheel slip.

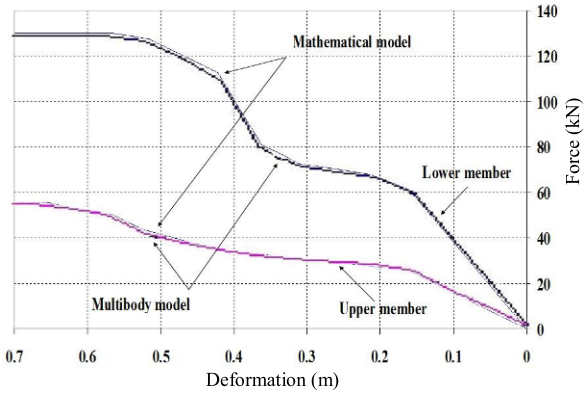

Figure 6. Force deformation characteristics for upper and lower rails.

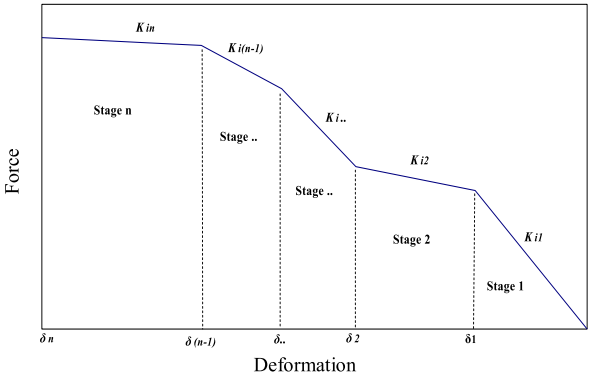

Figure 7. General piecewise force-deformation characteristics.

The vertical forces F_{zk} at each wheel can be written as follows:

$$F_{zfR} = m \cdot g \cdot \frac{l_r}{l} + F_{SfR} \tag{20}$$

$$F_{zfL} = m \cdot g \cdot \frac{l_r}{l} + F_{SfL} \tag{21}$$

$$F_{zrR} = m \cdot g \cdot \frac{l_f}{l} + F_{SrR} \tag{22}$$

$$F_{zrL} = m \cdot g \cdot \frac{l_f}{l} + F_{SrL} \tag{23}$$

The AS force elements are taken in parallel with the existing conventional suspension system and applied in the vertical direction. The maximum AS force is considered to be 2000 N on each wheel with the maximum suspension travel limit of 100 mm, taking into consideration the response time of the AS system.

2.4. Forces generated by the frontal nonlinear springs

To simulate the upper and lower members of the vehicle front structure, multi- stage piecewise linear force-deformation spring characteristics are considered. The non-linear springs used in the multi-body model [14] are taken to generate the n stage piecewise spring's characteristics, as shown in Figure 6. The forces of the front-end springs are calculated using the general relationship between the force and deflection of a nonlinear spring described in Figure 7 as follows:

$$Fs_i = k_{sij}\delta_i + F_{ij} \tag{24}$$

where k_s and δ represent the stiffness and the deflection of the front-end spring, respectively. The subscript i indicates the spring location (u_R: upper right spring, u_L: upper left spring, l_R: lower right spring and l_L: lower left spring) and the subscript j indicates different stages of the force-deformation characteristics as shown in Figure 7. The stiffness of the spring k_s and the force elements F_{ij} vary according to the different stages of the deflection δ and can be defined as follows:

$$k_{sij} = k_{si1}, \quad F_{ij} = 0 \quad 0 \le \delta < \delta_{i1} \tag{25}$$

$$k_{sij} = k_{si1}, \quad F_{ij} = (k_{si1} - k_{si2})\delta_{i1} \quad \delta_{i1} \le \delta < \delta_{i2} \tag{26}$$

$$\begin{gathered} k_{sij} = k_{si3}, \\ F_{ij} = (k_{si1} - k_{si2})\delta_{i1} + (k_{si2} - k_{si3})\delta_{i2} \\ \delta_{i2} \le \delta < \delta_{i3} \end{gathered} \tag{27}$$

$$\begin{gathered} k_{sij} = k_{\sin}, \\ F_{ij} = (k_{si1} - k_{si2})\delta_{i1} + (k_{si2} - k_{si3})\delta_{i2} + \ldots \\ + (k_{si(n-1)} - k_{sin})\delta_{i(n-1)} \\ \delta \ge \delta_{(n-1)} \end{gathered} \tag{28}$$

where the deformation of the front-end springs δ_i can be calculated using Figures 3 and 4(c) as:

$$\delta_{uR} = x + \delta_{\theta uR} + \delta_{\phi uR} - \delta_b \tag{29}$$

$$\delta_{uL} = x + \delta_{\theta uL} + \delta_{\phi uL} \tag{30}$$

$$\delta_{lR} = x + \delta_{\theta lR} + \delta_{\phi lR} - \delta_b \tag{31}$$

$$\delta_{lL} = x + \delta_{\theta lL} + \delta_{\phi lL} \tag{32}$$

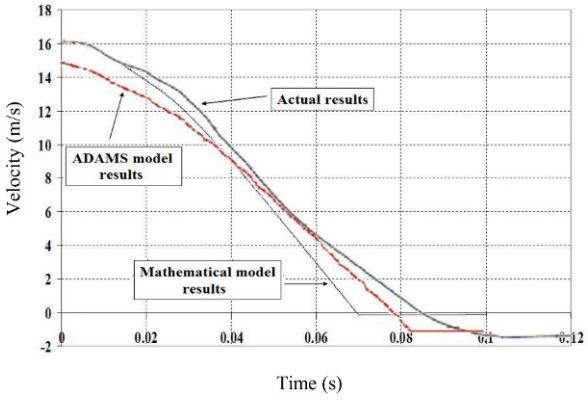

Figure 8. Velocity of the vehicle body.

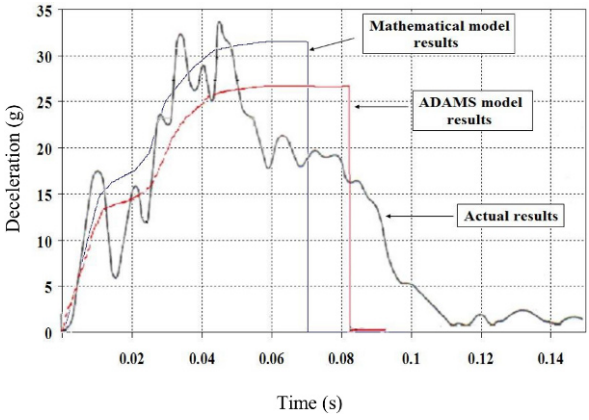

Figure 9. Deceleration of the vehicle body.

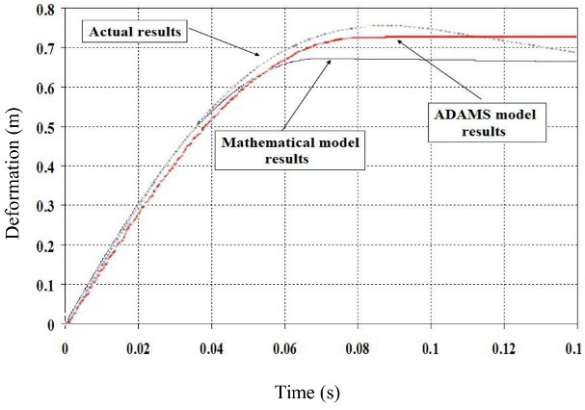

Figure 10. Deformation of the front-end structure.

where δ_θ, δ_ϕ and δ_b represent the deflection of the front end due to pitching, yawing and the bumper's rotation, respectively, and can be calculated as:

$$\delta_{\theta uR} = \delta_{\theta uL} = \sqrt{l_f^2 + e_1^2} \cdot \cos\left(\tan^{-1}\left(\frac{e^1}{l_f}\right) - \theta\right) - l_f \tag{33}$$

$$\delta_{\theta lR} = \delta_{\theta lL} = l_f - \left[\sqrt{l_f^2 + e_2^2} \cdot \cos\left(\tan^{-1}\left(\frac{e^2}{l_f}\right) + \theta\right)\right] \tag{34}$$

$$\delta_{\phi uR} = \delta_{\phi lR} = (l_a - x) - l_{\phi R} \tag{35}$$

$$\delta_{\phi uL} = \delta_{\phi lL} = l_{\phi L} - (l_a - x \tag{36}$$

$$l_{\phi L} = \frac{(l_a - x) + a_i \sin\phi}{\cos\phi} \tag{37}$$

$$\delta_b = \sqrt{(l_o - l_o \cos\phi_1)^2 + (l_o \cdot \sin\phi_1 + l_{\phi R} \cdot \cos\phi)^2} - l_{\phi R} \tag{38}$$

3. Car model validation

To ensure that the model is valid and provides accurate results of crumble zone deformation and the dynamic responses of the vehicle body are reliable, comparisons between the mathematical model, real test data and former multi-body model are established. In the real crash test, the vehicle was in free-rolling mode with an impact speed of 16.1 m/s; therefore the same conditions are used as initial conditions in the mathematical model simulation. The comparison of the mathematical model, ADAMS multi-body model [14] and real test results [18] are depicted in Figures 8–10. The lower initial speed of 15.1 m/s at the moment of impact of the ADAMS model as shown in Figure 8 is due to the effect of rolling resistance prior to impact [14], while the initial speed of the mathematical model is adapted to be the same as the actual test impact speed. However, the post-impact velocity curve of the mathematical model is in a good correlation with both real test and ADAMS model results.

In the vehicle body deceleration results shown in Figure 9, a high correlation between the mathematical model and the ADAMS model and the mean results of the real test is observed. The sudden reduction of the vehicle deceleration at the end of the collision on the mathematical model and ADAMS results is due to the deactivation of the spring forces at this point (there is no recoil of the springs). Although the mathematical model predicted a slightly higher value than the ADAMS results, the mean

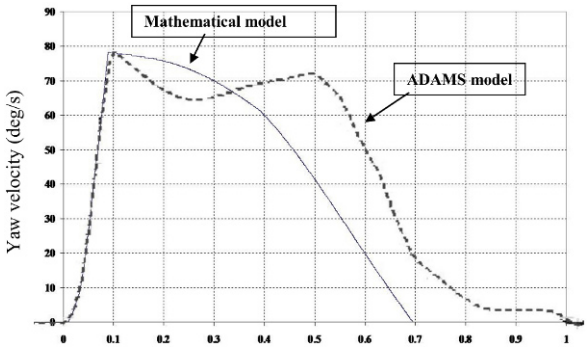

Figure 11. Yaw velocity of the vehicle body.

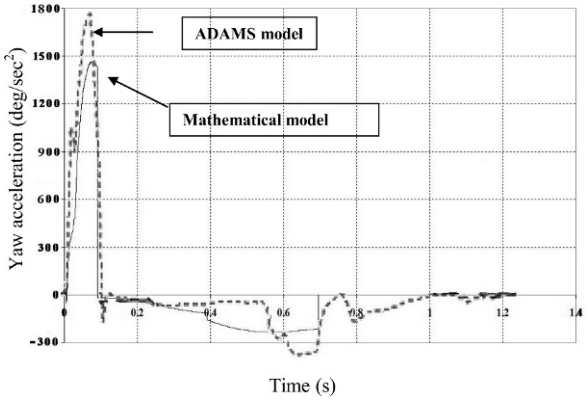

Figure 12. Yaw acceleration of the vehicle body.

value of deceleration is approximately the same as that of the actual results. The deformation of the front-end structure is illustrated in Figure 10, and a slightly lower value of the maximum deformation appeared in the mathematical model. This may be due to mass differences or other assumed parameters. However, the trend in the three cases is approximately the same with small differences in the maximum deformation.

Figures 11 and 12 show the comparison between the mathematical model results and the ADAMS results for vehicle yaw velocity and acceleration. In Figure 11 the vehicle velocities are almost the same in both models until they reach the maximum values (at the end of the crash). After the crash ended, the vehicle yaw is dependent on the maximum vehicle pitch angle and the period during which the rear wheels leave the ground. This describes the difference between the yaw velocity results of each model at post-crash. While the maximum vehicle yaw acceleration is slightly higher in the ADAMS model results than the mathematical model results, a good correlation between both results is noted as shown in Figure 12.

4. Prediction of the vehicle crash behaviour in different crash scenarios

In this section the vehicle crash performance is predicted when different cases of VDCS are applied at full and offset frontal collision scenarios. The following four cases have been chosen to fulfil this numerical study with full and offset frontal collision and five different speeds for each case (25, 40, 55, 70, and 85 km/hr):

- free rolling: in this case the vehicle collides with the barrier without applying any type of control;
- ABS: in this case the anti-lock braking system is applied before and during the collision;
- anti-pitch control system: the AS control is used to maintain the vehicle almost horizontal before the crash by applying an active force element on the front and rear wheels in upward and downward directions, respectively. A fuzzy control scheme is used to control the vehicle in this case;
- under-pitch control: here the vehicle has assumed a reverse pitching angle before crash using an AS control system; Fuzzy control is also used in this status.

While the ADAS detected that the crash will be unavoidable 1.5 s prior to the impact [4], VDCS will be applied in this short time preceding the impact. The values of the different parameters which were used in simulations are given in Table 1.

Table 1. The values of the different parameters which are used in the simulations.

Parameter	Value
m	1200 kg
I_{yy}	1490 kg·m^2
I_{xx}	350 kg·m^2
I_{zz}	1750 kg·m^2
I_{bzz}	40 kg·m^2
$k_{SfR} = k_{SfL}$	18.25 kN/m
$k_{SrR} = k_{SrL}$	13.75 kN/m
$c_{fR} = c_{fL}$	500 N·s/m
$c_{rR} = c_{rL}$	425 N·s/m
l_f	1.185 m
l_r	1.58 m
h	0.452 m
l_a	1.2 m
l_b	0.85 m
$b_i = b_o$	0.8 m

Table 2. Numerical results of a full frontal crash scenario VDCS and different five speeds.

Measured Data	Velocity (km/hr) / Case	25	40	55	70	85
Maximum deformation of the front-end (m)	Free Rolling	0.2422	0.4388	0.6309	0.8491	1.0895
	ABS	0.2306	0.4258	0.6187	0.8397	1.0798
	Anti-pitch Control	0.2309	0.4248	0.6181	0.8381	1.0798
	Under-pitch Control	0.2309	0.4247	0.6177	0.8368	1.0777
Maximum deceleration of the vehicle body (g)	Free Rolling	16.5988	25.5868	31.8283	36.0064	39.7748
	ABS	17.2676	25.4312	31.5362	35.7414	39.6217
	Anti-pitch Control	17.3548	25.8653	31.5831	35.8	39.6868
	Under-pitch Control	17.3548	25.9496	31.6441	35.8297	39.7053
Maximum pitch angle of the vehicle body (deg)	Free Rolling	3.562	6.5493	9.6528	12.8438	16.3658
	ABS	5.7222	10.2092	15.426	20.5462	26.2699
	Anti-pitch Control	2.7121	5.2219	7.6425	10.0766	12.904
	Under-pitch Control	1.0553	2.147	2.9148	3.2913	3.5714
Maximum pitch acceleration of the vehicle body (deg/s^2)	Free Rolling	842.193	1645.342	1907.999	2166.181	2505.821
	ABS	1127.298	2026.855	2376.793	3275.938	3950.203
	Anti-pitch Control	851.602	1439.692	1599.415	1755.704	2111.722
	Under-pitch Control	417.494	940.9045	992.9309	1002.639	1009.241

Note: The percentage of improvement is calculated related to the comparison between the values at case 4 with the others at case 1.

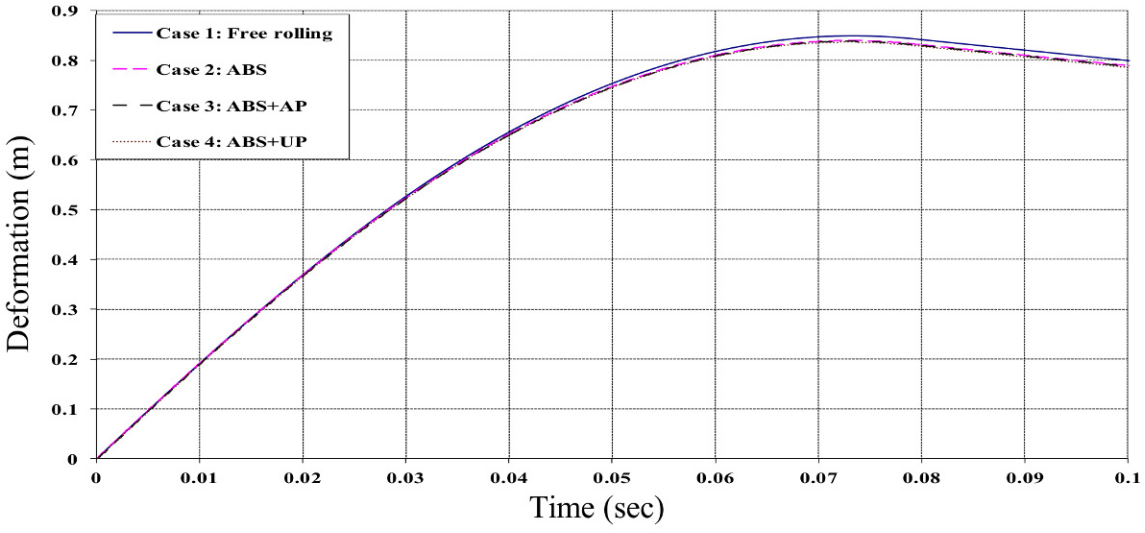

Figure 13. Deformation of the vehicle front-end for all cases at full frontal collision and speed of 70 km/hr.

4.1. Full frontal crash results

The deformation of the front-end structure, deceleration, pitch angle and acceleration of the vehicle body are determined in all four cases and five speeds as shown in Table 2. Five different speeds have been used to compare the effect of the applied control system at these diverse crash speeds. The speed of 70 km/hr has been chosen to illustrate the behaviour of the vehicle with the time which is similar on the other crash speeds. Figure 13 shows the front-end structure's deformation-time histories of all cases at this speed. Slight differences in the maximum deformation of the vehicle's front-end are found in each separate case; however, reduction in the maximum deformation is obtained when the ABS is applied (cases 2–4) with almost the same values.

Vehicle body deceleration – time histories for all cases are depicted in Figure 14, and it can be said that there is no significant difference in trends or values. However, in cases 2–4, when the ABS is applied, a very small change in the higher value of the vehicle body deceleration is observed at the early stage of crash in comparison to case 1 (free

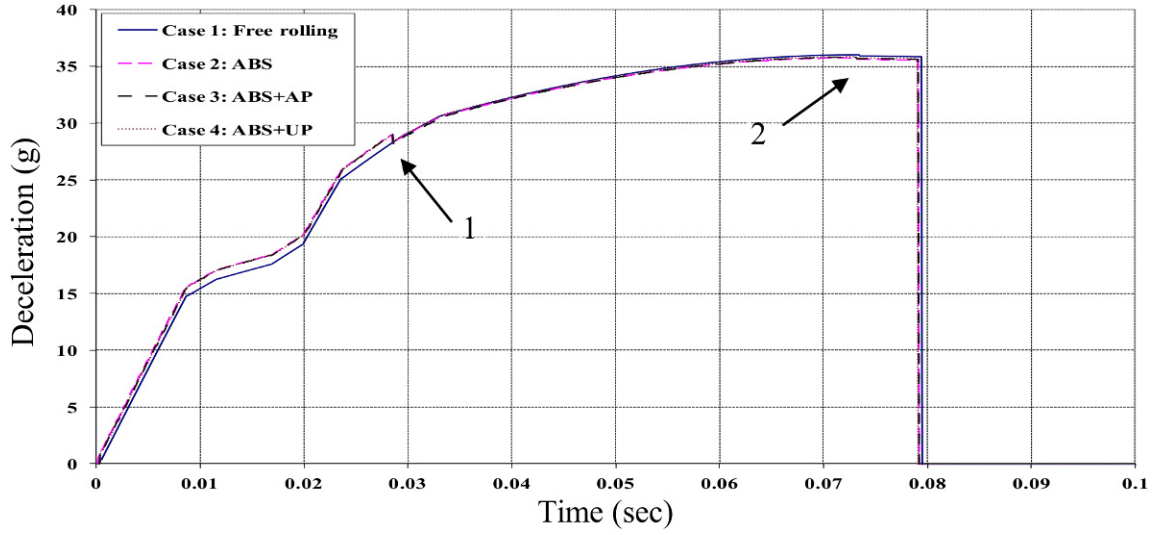

Figure 14. Deceleration of the vehicle body for all cases at full frontal collision and speed of 70 km/hr.

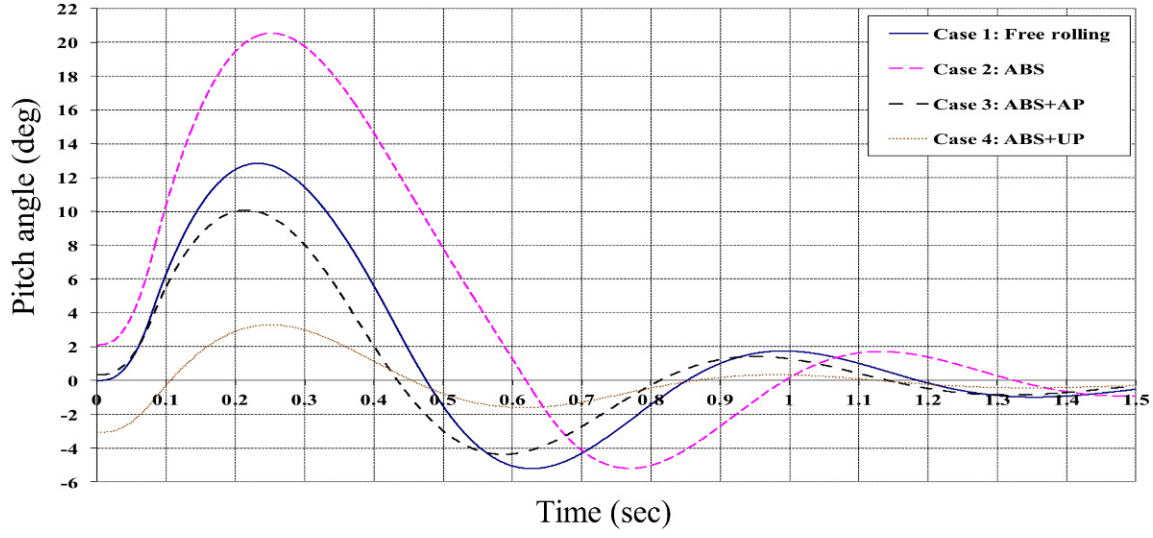

Figure 15. Pitch angle of the vehicle body for all cases at full frontal collision and speed of 70 km/hr.

rolling). These higher values exist until the front wheels reach the barrier and their braking effect ends; at this point rapid reduction in the vehicle body deceleration occurs (arrow 1, Figure 14). At the end of the collision the vehicle is stopped and starts moving in the opposite direction; meanwhile the braking force also changes its direction and deceleration is suddenly decreased as shown in Figure 14, arrow 2.

Figure 15 shows the vehicle pitch angle-time histories for all cases at the same speed (70 km/hr). The VDCS is applied 1.5 second before collision and, therefore, the vehicle body impacts with the barrier at different values of pitch angles related to each case as shown in the figure. The vehicle pitch angle then reaches its maximum values (normally after the end of crash) related to each case. Following this, the pitch angle is reduced to reach negative values and then bounces to reach its steady-state condition.

In the case of free rolling, vehicle body pitching angle is generated solely due to the different impact forces between the upper and lower front-end springs, while in case 2 (only ABS is applied) extra pitching moment is generated due to the braking force. This explains how the maximum pitch angle is observed in this case. In case 3 (ABS +

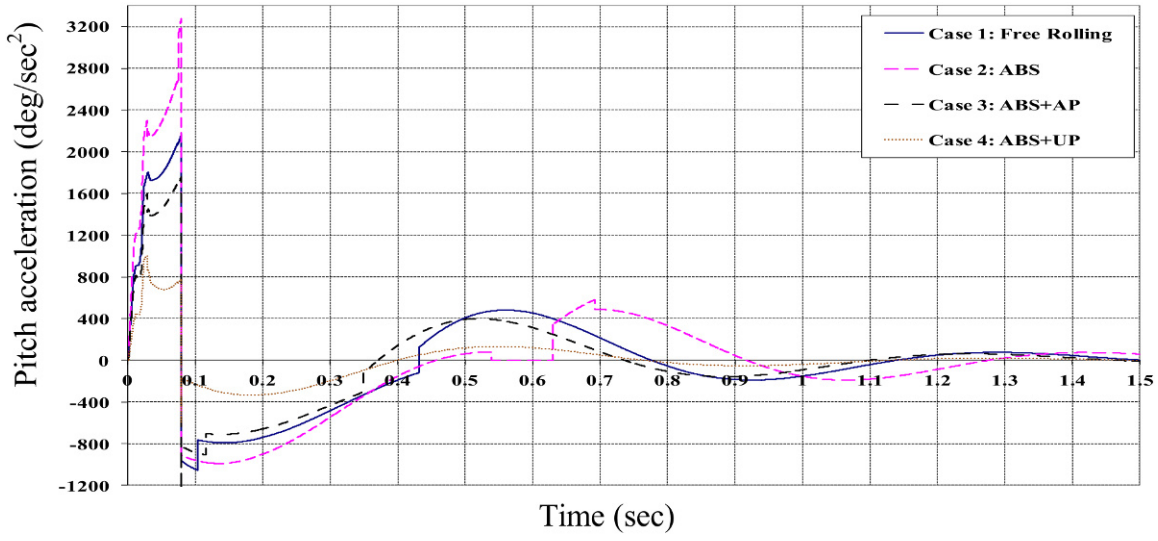

Figure 16. Pitch acceleration of the vehicle body for all cases at full frontal collision and speed of 70 km/hr.

AP), the AP control system helps the vehicle to reduce its pitching by generating pitching moment in the opposite direction; and that clarifies the reduction in the maximum vehicle body pitching in this case which is lower than the pitch angle in case 1. When the under pitch technique is applied along with ABS (case 4), the vehicle is given a negative pitch angle before impact, and the UP forces will generate a negative pitch moment before and during impact. In this case a great improvement of vehicle pitching is obtained an it can be seen from Table 2 that as the maximum pitch angle (at speed of 85 km/hr) is reduced from about 16 degree in the free rolling case to about 3.5 degrees (almost equal to the maximum pitching angle in the case of free rolling at speed of 25 km/hr, see Table 2). Comparing the effect of applying the UP control along with ABS (case 4) on vehicle crash at different impact speeds, it can be observed that the improvement of vehicle pitching is increased from about 70% at vehicle crash speed of 25, 40 and 55 km/hr to about 74% at 70 km/hr and 78% at 85 km/hr (see Table 2).

Vehicle pitch acceleration-time histories are depicted in Figure 16 for all four cases. The pitch acceleration is increased very fast at the early stage of crash, and then it is increased rapidly at the lower rate to reach its maximum value for each case due to the high pitching moment that is generated from the collision. At the end of the collision, all pitching moment due to the crash is equals zero; vehicle speed is negative with very low value, and the vehicle pitch angle is still positive. That means the vehicle is now controlled by the tyres and suspension forces which have already generated moment in the opposite direction of vehicle pitching. That describes the reason for the high drop and the changing direction from positive to negative on the vehicle pitch acceleration at the end of the crash. As shown in the figure the vehicle maximum pitching acceleration occurs at the end of collision and the greatest value of the maximum pitching acceleration is observed in case 2 (ABS) whilst the lowest value is detected in case 4 (ABS + UP). The reduction of the vehicle pitch acceleration in case 4 is also notable; it decreases from about 2500 deg/s^2 in case of free rolling to about 1000 deg/s^2 at speed of 85 km/hr (see Table 2). The percentage of enhancement of vehicle pitching acceleration is increased from about 50% at vehicle crash speeds of 25, 40 and 55 km/hr to about 54% at 70 km/hr and 60% at 85 km/hr as observed from Table 2.

4.2. Offset crash results

In an offset crash scenario, the deformation of the impacted side of the front-end structure, deceleration, pitch angle and acceleration of the vehicle body as well as the yawing angle, velocity and acceleration of the vehicle body are obtained in all four cases and five speeds as shown in Table 3. The vehicle front-end deformation at a speed of 85 km/hr exceeds the allowable length of the frontal structure (1.2 m), and that means the compartment has been intruded. The speed of 70 km/hr is also chosen to illustrate the results of the offset collision.

Figure 17 shows the impacted side of the front-end structure's deformation-time histories of all cases at speeds of 70 km/hr. Logically, the maximum deformation of the front-end in an offset crash is greater than the one in full crash because most of the crash energy is absorbed by

Table 3. Numerical results of an offset frontal crash scenario with different cases of VDCS and different five speeds.

Measured Data	Velocity (km/hr) / Case	25	40	55	70	85
Maximum deformation of the front-end (m)	Free Rolling	0.292	0.5264	0.778	1.0588	1.3846
	ABS	0.2745	0.5032	0.751	1.0309	1.3465
	Anti-pitch Control	0.2721	0.5012	0.7484	1.029	1.3467
	Under-pitch Control	0.2718	0.501	0.7478	1.0269	1.3442
Maximum deceleration of the vehicle body (g)	Free Rolling	14.0494	20.8693	24.0283	25.9726	26.8992
	ABS	14.5286	20.9743	24.1507	26.3929	27.3878
	Anti-pitch Control	14.7553	21.3356	24.5259	26.4515	27.4686
	Under-pitch Control	14.7569	21.3887	24.5521	26.4064	27.4406
Maximum pitch angle of the vehicle body (deg)	Free Rolling	3.4484	6.3885	8.9448	12.2006	15.799
	ABS	5.5888	9.8968	14.447	19.9578	26.035
	Anti-pitch Control	2.1586	4.6844	6.8887	8.8666	11.6186
	Under-pitch Control	0.9107	1.91	2.4075	2.8667	3.15
Maximum pitch acceleration of the vehicle body (deg/s^2)	Free Rolling	639.9765	1156.753	1293.902	1412.786	1403.893
	ABS	858.2273	1481.893	1718.977	2305.751	2553.295
	Anti-pitch Control	461.5038	974.2194	1327.907	1124.741	1213.729
	Under-pitch Control	309.3607	617.1925	617.3229	640.2067	664.8851
Maximum yaw angle of the vehicle body (deg)	Free Rolling	2.5547	16.2817	46.2297	106.3904	258.4531
	ABS	2.9244	15.9719	47.5325	110.9078	256.805
	Anti-pitch Control	2.2525	13.0993	36.8748	86.7191	207.3422
	Under-pitch Control	1.4086	10.1154	30.9308	75.2819	179.1226
Maximum yaw acceleration of the vehicle body (deg)	Free Rolling	320.7683	949.0331	1590.851	2514.016	3909.887
	ABS	333.8712	899.4895	1525.85	2406.812	3756.187
	Anti-pitch Control	348.9306	879.1682	1475.742	2399.165	3705.266
	Under-pitch Control	310.9987	837.1089	1455.512	2377.743	3635.358

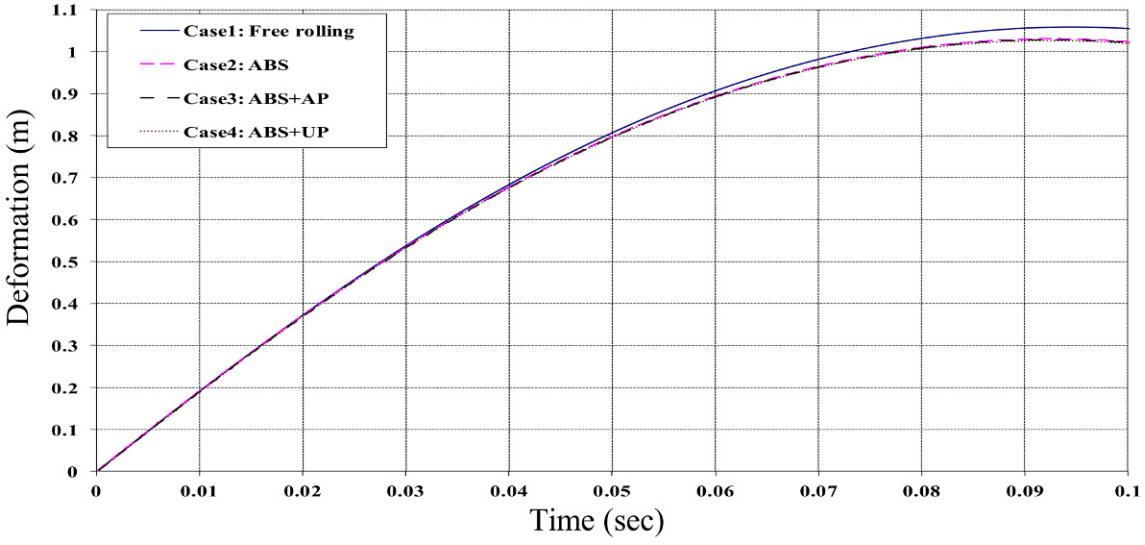

Figure 17. Time (sec) Deformation of the vehicle front-end for all cases at offset collision and speed of 70 km/hr.

one side of the vehicle. Similarly as observed in a full crash, slight differences in the maximum deformation of the vehicle's impacted side are found in the four different cases of offset crash; however the minimum deformation is obtained in case 4. In this case a reduction of about 30 mm is obtained compared with the free rolling case.

Vehicle body deceleration – time histories for all cases are depicted in Figure 18 and it found that there is no significant difference in trends or values. The fast reduction in the vehicle body deceleration (arrow 1 in Figure 18) occurs when the front left wheel reaches the barrier and its braking effect is ended. Additionally, at the end of

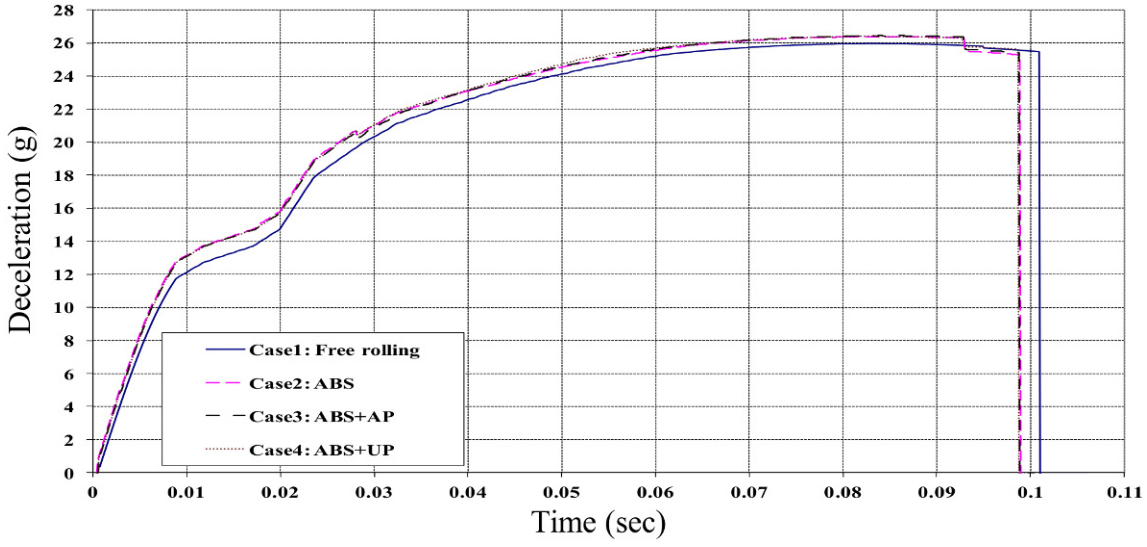

Figure 18. Deceleration of the vehicle body for all cases at offset collision and speed of 70 km/hr.

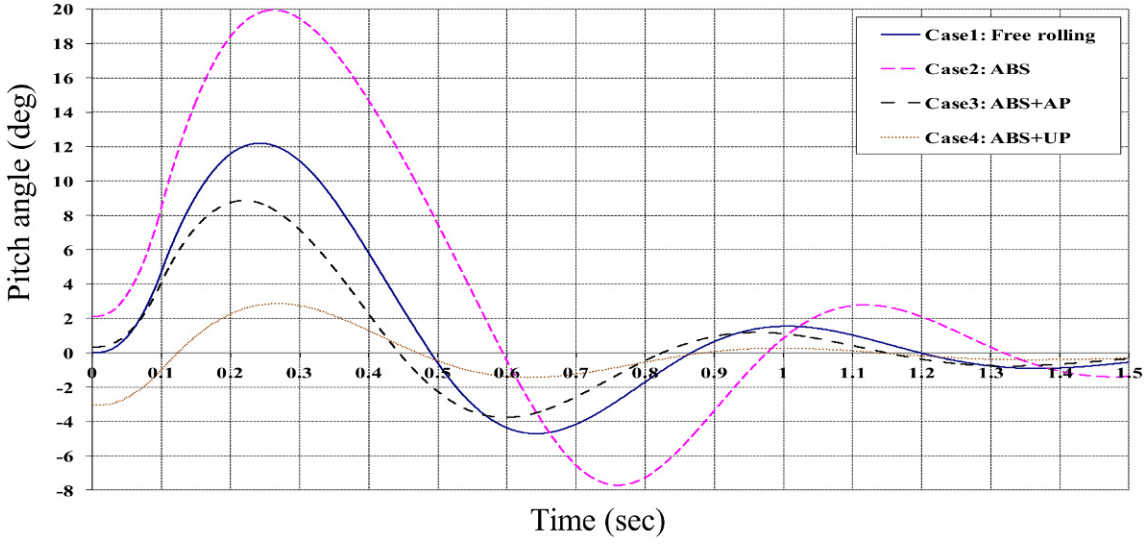

Figure 19. Pitch angle of the vehicle body for all cases at offset collision and speed of 70 km/hr.

the collision the vehicle is stopped and starts moving in the opposite direction meanwhile the braking force also changes its direction and deceleration is suddenly decreased as shown in Figure 18, arrow 2.

Figure 19 shows the vehicle pitch angle-time histories for all cases. Similar to the full crash scenario, different values of pitch angles at the point of impact are shown related to each case because the VDCS is applied 1.5 second before collision. The maximum pitch angle is observed in case 2, and this is due to the pitching moment that is generated because of the braking force as mentioned in the case of a full crash. Similar to the full crash scenario, the minimum pitch angle is obtained when the UP control system is applied along with the ABS. Furthermore a great improvement of vehicle pitching is obtained as the maximum pitch angle is reduced from about 12 degree in the free rolling case to about 3 degrees at this case. Comparing the effect of applying the UP control along with the ABS (case 4) to the vehicle crash at different impact speeds, it can be observed that the improvement of vehicle pitching is increased from about 73% at different crash speeds to about 76.5% at 70 km/hr (see Table 3).

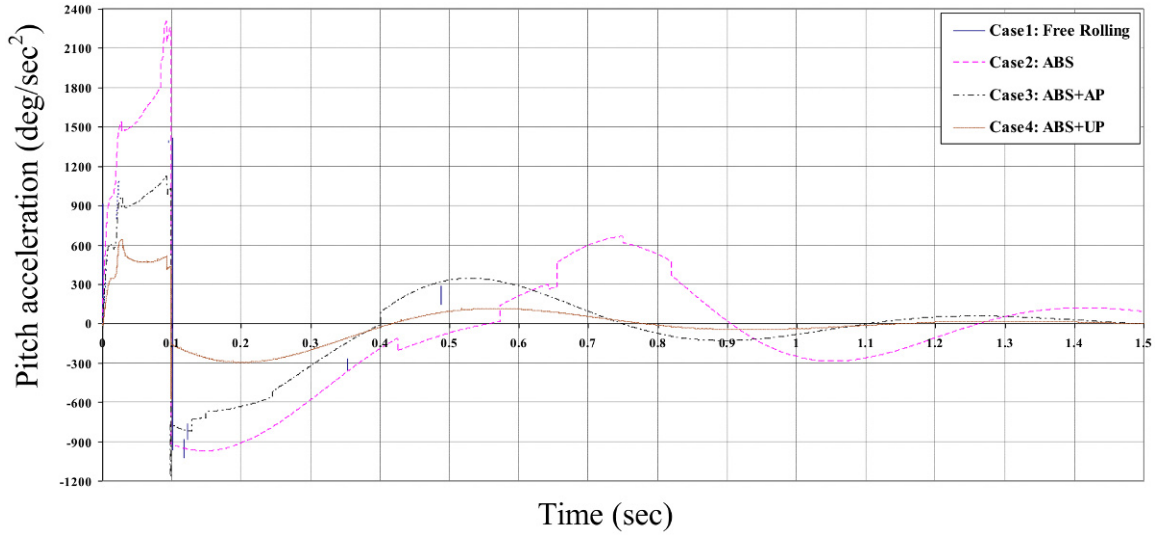

Figure 20. Pitch acceleration of the vehicle body for all cases at offset collision and speed of 70 km/hr.

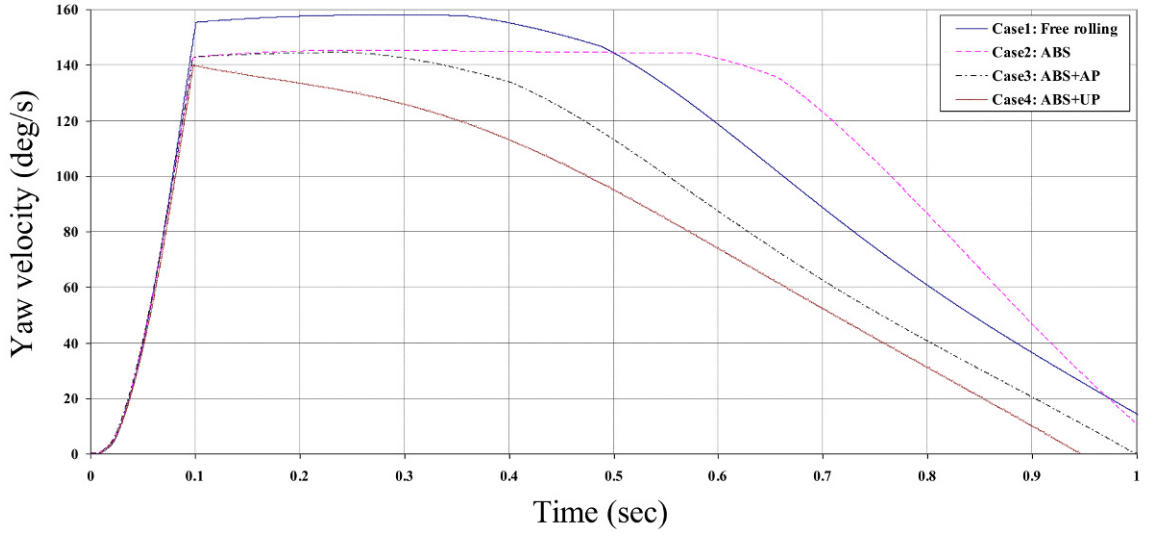

Figure 21. Yaw velocity of the vehicle body for all cases at offset collision and speed of 70 km/hr.

Vehicle pitch acceleration-time histories are depicted in Figure 20 for all four cases. The greatest value of the maximum pitching acceleration is also detected in case 2 (ABS) while the lowest value is observed in case 4. The reduction of the vehicle pitch acceleration is also notable in offset crash scenario; it decreases from about 1400 deg/s^2 in case of free rolling to about 640 deg/s^2 in this case. The percentage of enhancement of vehicle pitching acceleration is increased from about 51% at the different crash speeds to about 54% at 70 km/hr (see Table 3).

In the offset collision, only one side of the vehicle is impacted, which creates a high difference between the right and left front-end springs' forces, and that is the main source of the yaw moment that makes the vehicle body rotate around the z axis. Figure 21 shows the vehicle yaw velocity-time histories for all cases at the same vehicle collision speed of 70 km/hr. Vehicle yaw velocity is equal to zero before the crash then it is changed in three different stages: firstly it is increased rapidly during the collision; secondly it is changed slowly to reach a specific value; and thirdly it is decreased gradually to reach zero value. In the first stage, the rapid increase in the yaw velocity is due to the high acceleration (see Figure 22) caused by the one sided impacted spring. At the end of the collision, the

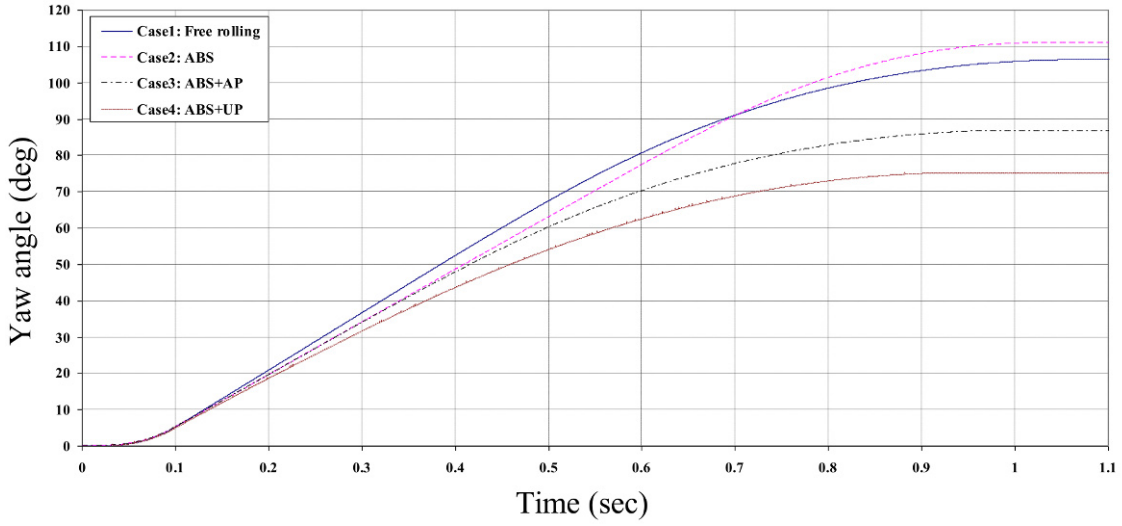

Figure 22. Yaw angle of the vehicle body for all cases at offset collision and speed of 70 km/hr.

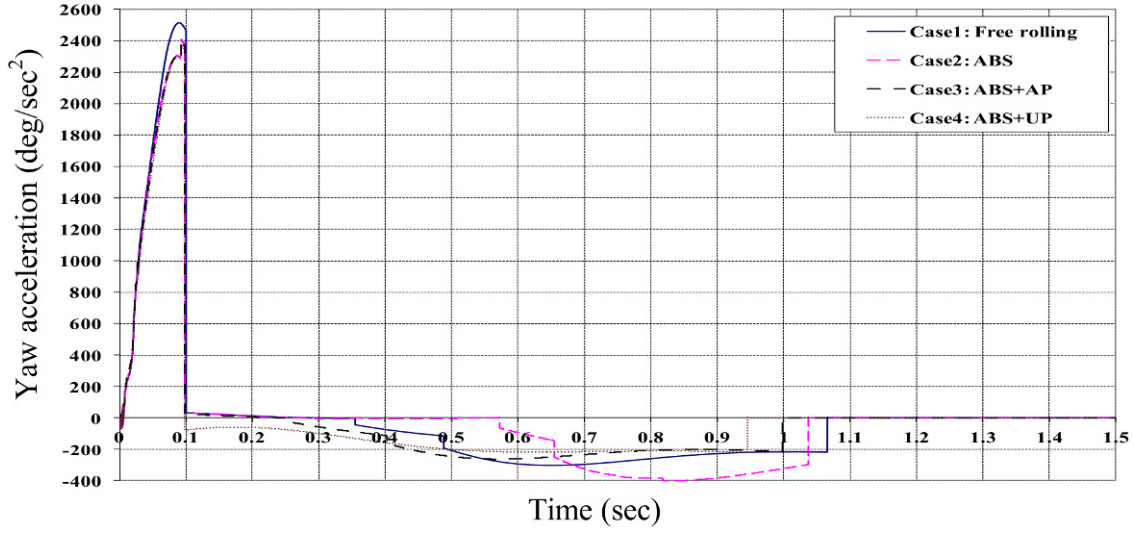

Figure 23. Yaw acceleration of the vehicle body for all cases at offset collision and speed of 70 km/hr.

rear wheels have already left the ground due to the vehicle pitching and the vehicle is now controlled by the front wheels alone. So, in the second stage, the decrease in the vehicle's yaw velocity is due to the friction force between the front tyres and the ground. Stage 3 begins when the rear wheels initiate contact with the ground which generates yaw moment in the opposite direction causing a reduction of the vehicle yawing velocity at a higher rate than the decreasing velocity rate in the second stage. It should be noted that at low speeds the rear wheels do not leave the ground and stage 2 is not existed.

Because of the maximum vehicle front-end deformation observed in case 1 (free rolling), as shown in Figure 17, the greatest peak of yaw velocity appears in the same case, as shown in Figure 21. The maximum yaw velocities are approximately the same for case 2 and 3, and the maximum velocity of case 4 is the lowest. The period of the second stage is different for each case and is mainly dependent on pitching angle and the time that the rear wheels leave the ground. It is monitored because, in case 4, the rear wheels do not leave the ground.

Figure 22 shows the vehicle body yaw angle-time histories for all cases. While the maximum yaw velocity and acceleration (Figures 21 and 23) occur at case 1 (free rolling), It is found that the maximum yaw angle of about 111 degrees is noted in case 2 (ABS). That is because the

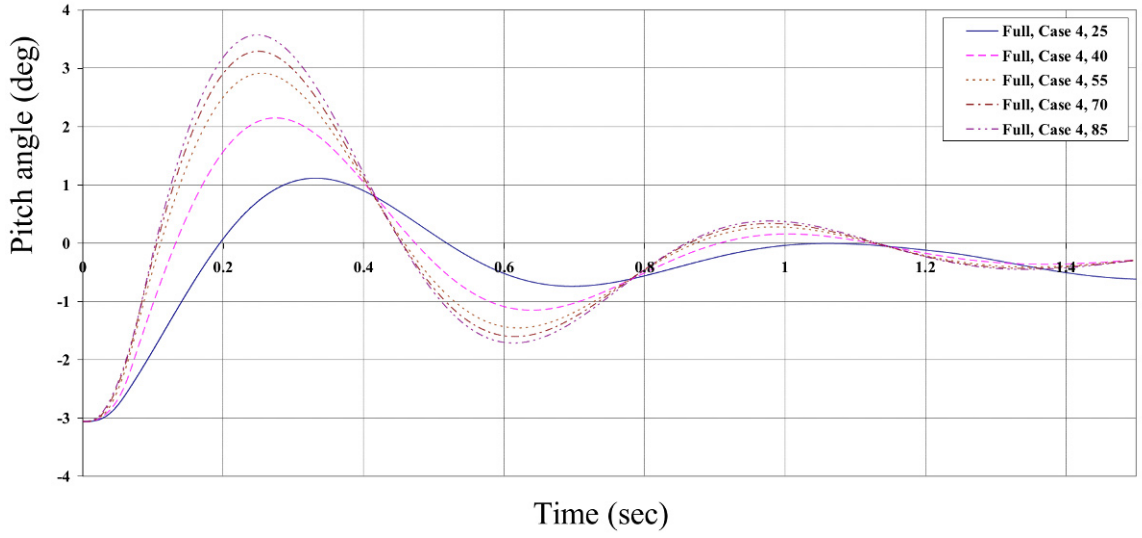

Figure 24. Pitch angle of the vehicle body at the different five speeds with case 4.

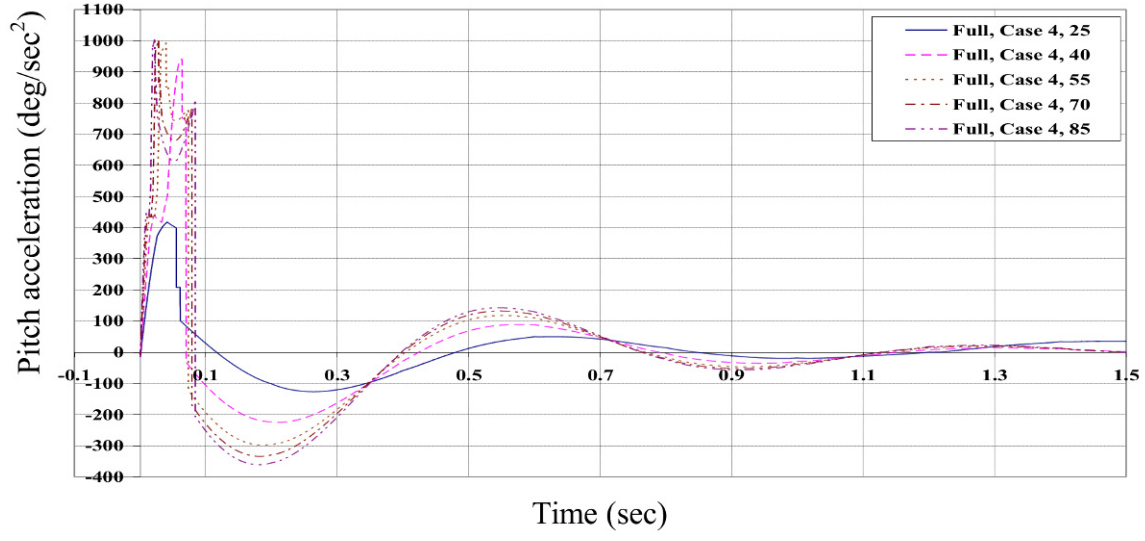

Figure 25. Pitch acceleration of the vehicle body at the different five speeds with case 4.

maximum value of the vehicle yaw angle is not depends only on the yaw acceleration, but it also depends on the vehicle pitch angle and the period of time that the rear wheels leave the ground for each case. The minimum yaw angle of about 75 degrees is noted in case 4 when the UP control is applied along with the ABS, and a reduction of about 36 degrees (32%) is obtained in this case compared with the ABS alone being applied. As described before, the UP technique is used to make the vehicle pitching up for a few degrees before the crash.

Vehicle body yaw acceleration-time histories are depicted in Figure 23. Maximum yaw acceleration is discovered in case 1 (free rolling), and yaw acceleration for the other cases is approximately the same. At the end of the collision the vehicle is controlled by the front wheels only, as mentioned before, which try to hinder the yawing motion; the negative acceleration is shown with different small values related to each case. These negative values of the vehicle yaw acceleration are changed slowly with time; then they reach zero rapidly when the yaw velocity equals zero.

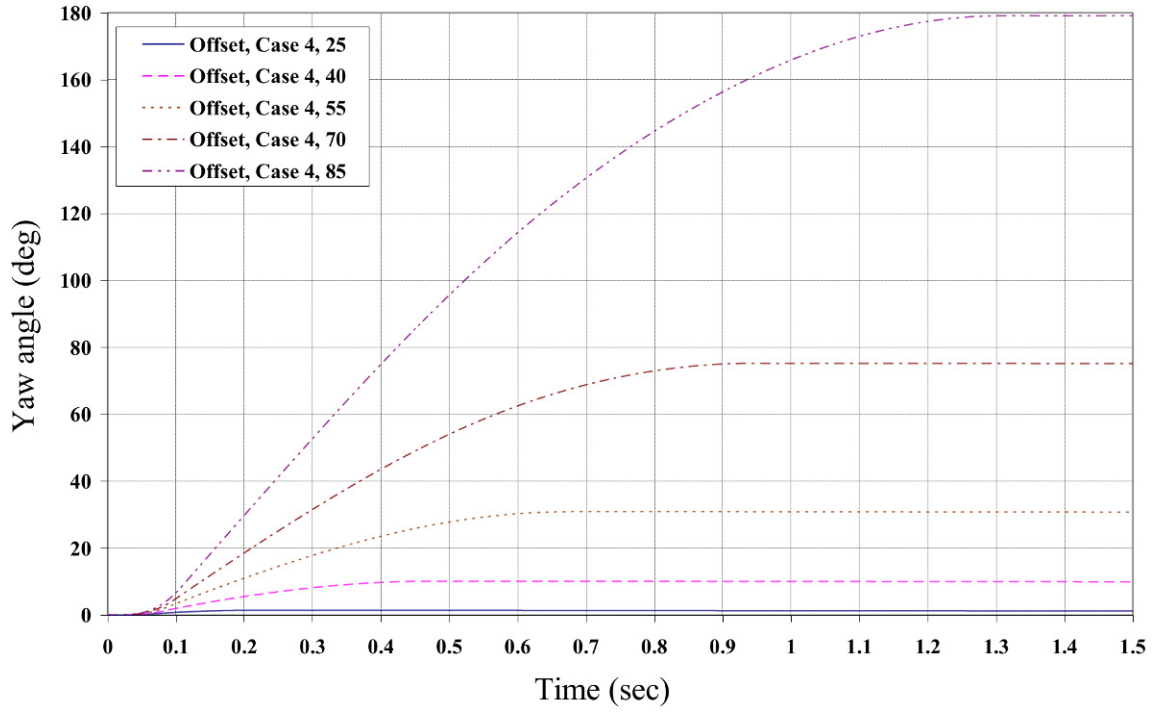

Figure 26. Yaw angle of the vehicle body at the different five speeds with case 4.

4.3. The effect of the UP control (case 4) on the crash speed

While the effect of the UP control on the vehicle front-end deformation and deceleration is small, the vehicle pitching event is used to show the relation between the UP control technique with the different crash speeds. Figure 24 shows the vehicle pitch angle at the different crash speeds when the UP control is applied along with ABS at full frontal collision. From this figure it can be observed that the relation between the increase of crash speed and the effect of the UP control is not linear, which is not detected on the other three cases (case 1, 2 and 3). In other words, when the crash speed is increased from 25 to 40 (km/hr), the incremental of the maximum pitch angle is equal to 1.09 deg.; and with the increase of the crash speed, the incremental of the maximum pitch angle is decreased. For example, when the crash speed is increased from 70 to 85 (km/hr), the incremental of the maximum pitch angle is equal to 0.28. This nonlinear relation means that the efficiency of the UP control system is increased with the crash speed. Figure 25 shows the pitch acceleration-time histories for all different speeds in full frontal collision when the case four is applied. It is observed here that in addition to nonlinearity of the relation between the effect of UP control and the vehicle crash speed, the maximum pitch accelerations at speeds of 55, 70, and 85 (km/hr) are almost the same. This results indicates the robustness of the UP control technique at high crash speeds.

The same nonlinear effect of the UP control system on vehicle pitching is also noticed in offset crash scenarios with different values. Figure 26 shows the vehicle yaw angle-time histories for all different five speeds in offset frontal crash when the case four is applied. It is observed that the relation between the effect of the UP control system on vehicle yawing is also nonlinear, but in opposite manner. In other words, when the crash speed is increased, the incremental of the maximum yaw angle is increased. This nonlinear relation is also observed on the vehicle yaw velocity and acceleration; in addition, it is noticed on the other three cases (case 1, 2, and 3). So it can be said that while the UP control helps to reduce the maximum vehicle yaw angle and velocity, its effect is not increased at high speed crashes.

From this study of full frontal and offset crash scenarios, it can be said that the vehicle pitch angle and acceleration are greatly reduced when the ABS is applied with the UP control. There are two notable benefits of reducing the vehicle pitching. Firstly, it makes the crash event more survivable even considering the risk of head and neck injury as stated by Chang *et al.* [7]. Secondly, reducing the vehicle pitching is the main reason for decreasing the

maximum yaw angle. The benefit of the reduction of the maximum yaw angle is to lessen the risk of the car being side-impacted by any obstacles on the road.

5. Conclusion

Development of a new 6-DOF vehicle dynamics/crash mathematical model has been employed to study the effect of vehicle dynamic control systems (VDCS) on high-speed vehicle crashes. The model presented here is validated against former model and real crash results; it would be very useful in the early design stages for assessing the crash worthiness of the vehicle. In this study, three different cases of VDCS have been used to enhance the vehicle behaviour at high-speed crash scenarios. The results show that the effect of the active VDCS is quite minimal in terms of vehicle deformation and deceleration; however, there are significant improvements on vehicle pitch event at full frontal collision. In addition, a noteworthy enhancement of vehicle pitching and yawing is observed at vehicle offset crash scenarios.

Acknowledgments

The authors would like to thank the Egyptian Government and the Faculty of Engineering, Ain Shams University for supporting this research. We also acknowledge, with sadness, the contribution of Prof. Dave Crolla who has passed away during the period of this research.

References

[1] SWOV Fact Sheet (2009), The Relation between Speed and Crashes, Insurance Institute for Highway Safety IIHS, Leidschendam, the Netherlands (http://www.swov.nl/rapport/Factsheets/UK/FS_Speed.pdf).

[2] Seiler P., Song B., Hedrick J.K., Development of a Collision Avoidance System, SAE International Congress & Exposition, Detroit, MI, USA, Paper No. 980853, 1998

[3] Tamura M., Inoue H., Watanabe T., Maruko N., Research on a Brake Assist System with a Preview Function, SAE World Congress, Detroit, MI, USA, Paper No. 2001-01-0357, 2001

[4] Jansson J., Gustafsson F., Johansson J., Decision Making for Collision Avoidance Systems, SAE World Congress & Exhibition, Detroit, MI, USA, Paper No. 2002-01-0403, 2002

[5] Schoeneburg R., Breitling T., Enhancement of Active & Passive Safety by Future Pre-safe Systems, Proceedings of the 19th ESV Conference, Washington, D.C., USA, 2005

[6] Gietelink O., Ploeg J., De Schutter B., Verhaegen M., Development of advanced driver assistance systems with vehicle hardware-in-the-loop simulations, Vehicle System Dynamics, vol. 44, no. 7, 2006, 569–590

[7] Chang J.M., Rahman M., Ali M., El-Bkaily M., *et al.*, Modeling and Design for Vehicle Pitch and Drop of Body-on Frame Vehicles, SAE World Congress & Exhibition, Detroit, MI, USA, Paper No. 2005-01-0356, 2005

[8] Chang J.M., Ali M., Craig R., El-bkaily M., *et al.*, Important Modeling Practices in CAE Simulation for Vehicle Pitch and Drop, SAE World Congress & Exhibition, Detroit, MI, USA, Paper No. 2006-01-0124, 2006

[9] Chang J.M., Huang M., Tyan T., Li G., *et al.*, Structural Optimization for Vehicle Pitch and Drop, SAE World Congress & Exhibition, Detroit, MI, USA, Paper No. 2006-01-0316, 2006

[10] Alleyne A., Improved Vehicle Performance Using Combined Suspension and Braking Forces, Vehicle System Dynamics, 27, 1997, 235-265

[11] Yue C., Butsuen T., Hedrick J.K., Alternative Control Laws for Automotive Active Suspensions, ASME Journal of Dynamics Systems, Measurement and Control, 111, 1989, 286–290

[12] Ting W.E., Lin J.S., Nonlinear Control Design of Anti-lock Braking Systems Combined with Active Suspensions, 5th Asian Control Conference, Melbourne, Australia, 2004

[13] Mastandrea M., Vangi D., In[U+FB02]uence of Braking Force in Low-speed Vehicle Collisions, Proceedings IMechE, 219, 2005, 151–164

[14] Hogan I., The Use of Vehicle Dynamic Control Systems for Automotive Collision Mitigation, PhD thesis, Department of Engineering and Technology, Manchester Metropolitan University, UK, 2008

[15] Emori R.I., Analytical Approach to Automobile Collisions, SAE World Congress & Exhibition, Warrendale, USA, Paper No. 680016, 1968

[16] Kamal M.M., Analysis and Simulation of Vehicle to Barrier Impact, SAE World Congress & Exhibition, USA, Paper No. 700414, 1970

[17] Khattab A., Investigation of an Adaptable Crash Energy Management System to Enhance Vehicle Crashworthiness, PhD thesis, the Department of Mechanical and Industrial Engineering, Concordia University, Canada, 2010

[18] TRL (1995), Real Crash Test Data. Obtained through the Internet: http://www.trl.co.uk